Algorithms for Tomographic Reconstruction of Rectangular Temperature Distributions using Orthogonal Acoustic Rays

Chuyoung Kim

Thesis submitted to the faculty of the Virginia Polytechnic Institute and State University in partial fulfillment of the requirements for the degree of

Master of Science

In

Mechanical Engineering

Wing F. Ng, Chair

K. Todd Lowe, Co-Chair

Alfred L. Wicks

Srinath V. Ekkad

August 5th, 2016

Blacksburg, VA

Keywords: Acoustic Thermometry, Non-intrusive Measurement, Tomography Reconstruction, Least Squares Method, Multiplicative Algebraic Reconstruction Technique

Algorithms for Tomographic Reconstruction of Rectangular Temperature Distributions using Orthogonal Acoustic Rays

Chuyoung Kim

Abstract

Non-intrusive acoustic thermometry using an acoustic impulse generator and two microphones is developed and integrated with tomographic techniques to reconstruct temperature contours. A low velocity plume at around 450 ℉ exiting through a rectangular duct (3.25 by 10 inches) was used for validation and reconstruction. 0.3 % static temperature relative error compared with thermocouple-measured data was achieved using a cross-correlation algorithm to calculate speed of sound. Tomographic reconstruction algorithms, the simplified multiplicative algebraic reconstruction technique (SMART) and least squares method (LSQR), are investigated for visualizing temperature contours of the heated plume. A rectangular arrangement of transmitter and microphones with a traversing mechanism collected two orthogonal sets of acoustic projection data. Both reconstruction techniques have successfully recreated the overall characteristic of the contour; however, for the future work, the integration of the refraction effect and implementation of additional angled projections are required to improve local temperature estimation accuracy. The root-mean-square percentage errors of reconstructing non-uniform, asymmetric temperature contours using the SMART and LSQR method are calculated as 20% and 19%, respectively.

Algorithms for Tomographic Reconstruction of Rectangular Temperature Distributions using Orthogonal Acoustic Rays

Chuyoung Kim

General Audience Abstract

Computational tomography is an approach to reconstruct the cross-sectional planar image of a 3D object. This technique is widely used in the medical field using x-rays to visualize cross-sections of internal organs. Along with x-rays, acoustic rays can also be utilized with tomographic techniques. The speed of sound travelling through a gaseous medium, such as air, is depended on the density, humidity, and temperature of the medium. Using this relationship, the temperature of the medium can be calculated with known speed of sound, density, and humidity. The speed of sound can be found using the distance and time of flight of the acoustic ray using transmitter and microphones. Since the effect of density and humidity of the medium on speed of sound is relatively insignificant, those values were assumed to be constant. In this research, the acoustic temperature measuring technique using the speed of sound relationship was applied and validated, then the technique was integrated with tomography using two projection angles. A rectangular duct (3.25 by 10 inches) with a heated air at around 450 °F exiting the duct was tested. The calculated temperature from acoustics was compared with values measured with thermocouples. After the acoustic temperature measuring technique was validated, multiple acoustic rays arranged in two orthogonal projections were setup. The speed of sound values from the acoustic rays were utilized to reconstruct the temperature distribution of the duct exit using two tomographic reconstruction methods: LSQR and SMART. Both reconstruction techniques have captured overall contour of the temperature. More projection angles and sound refractive properties will be utilized in the future to overcome the limitations of detailed reconstruction.

Acknowledgments

I would like to first thank Dr. Wing Ng and Dr. Srinath Ekkad for offering me a position to conduct graduate research at Virginia Tech. In this special opportunity, I was able to learn and develop an acoustic thermometry tomographic model, which was also made possible by my co-advisor, Dr. Todd Lowe. His advice and mentorship made this endeavor a unique experience for which I am very grateful. I would also like to thank Dr. Alfred Wicks for his advices on signal processing and efforts in serving on my committee. Their knowledge and expertise contributed to my development, as well as many other students at Virginia Tech.

Thank you to all of my friends and colleagues who were a part of my education. I am particularly indebted to Raul Otero Jr. for his collaboration and teaching. Dr. Wickersham and Dr. Ecker dedicated time to the design and development of the experimental test rig used for my research. Many thanks to the other VT researchers who have helped me over the past two years, including Suhyeon Park, David Mayo, Andrew Boulanger, Kris Barboza, Kartikeya Tyagi, Dan Cadel, and Jaideep Pandit. You assisted my work in many ways, making my graduate education an enjoyable and fulfilling experience.

On behalf of our entire research group, thank you to Rolls Royce for your sponsorship and involvement. In particular, I would like to thank Ed Hodge, Vic Oschel, Loren Crook, Raul Vasquez, and Fred Smith. We look forward to continued partnership in the future.

Finally, I must thank my family for encouraging me to pursue this opportunity and supporting me along the way. My parents in Korea and America helped financially, my siblings helped by visiting and encouraging.

Table of Contents

List of Figures

List of Tables

1. Introduction

1.1 Motivation

As the demand for commercial and military aircraft increase, various methods to monitor engine exit flow conditions are under development. In-flight monitoring of engine exhaust properties, such as velocity and temperature, is crucial for the performance and maintenance of jet engines. Most conventional methods used for the temperature monitoring of the engine exhaust plume are intrusive methods utilizing thermocouples. However, the direct insertion of equipment disturbs the flow and risks measurement inaccuracy from relatively slow time response and flow disturbance [1]. Due to the inaccuracy and cost of intrusive methods, non-intrusive methods, such as infrared and laser pyrometry, are frequently used. Both techniques have limitation since transparent windows for observation of light waves are required and are inaccurate when windows are contaminated [2, 3]. An acoustic thermometry method with transmitters and microphones was considered in this work as a promising non-intrusive approach to engine exhaust temperature monitoring. For the future, acoustic thermometry will be implemented as a thrust measurement technique integrated with recently developed acoustic velocimetry [4].

1.2 Background Review

The phenomenon of the change in speed of sound with the change in gas medium properties has been noticed and studied since the time of Galileo. Recorded experiments motivated by interest in the relationship between speed of sound and temperature is found as early as 1875, conducted by John Tyndall [5]. Since then, the change in acoustic properties through the medium has been studied and applied in the development of SONAR (SOund Navigation and Ranging), ultrasonic distance measurements, and other distance measuring techniques [6, 7].

Applications of acoustic measurements have diversified in various fields as tomographic reconstruction techniques have emerged. Sonography, commonly known as ultrasound, has been implemented into not only medical fields, but also into meteorology and oceanography using large scale acoustic tomographic techniques [8, 9, 10]. Tomographic techniques integrated with acoustic thermometry have been developed and applied for monitoring boilers and furnace temperature [11, 12]. A single acoustic ray projection has also been utilized to measure temperature of gas turbines and jet engines [13], but further steps were

taken as Siemens successfully measured and reconstructed the temperature profiles of ground gas turbine exhaust using acoustic thermometry and tomographic techniques. With 8 transceivers mounted on a circular frame around a turbine exit, temperature was measured within 10 ℃. A straight acoustic ray path line without refraction effect was assumed for the temperature measurement [14].

Siemens also demonstrated ground gas turbine exhaust measurement with improvement of signal-to-noise-ratio (SNR) of the sound source by using chirping transmitter was accomplished [15]. Using six pairs of transmitters and receivers, the bulk mean temperature of the exhaust at around 600 ℃ was measured within 0.36% compared with thermocouple measurement after applying correction for the velocity effect.

While the reconstructed temperature contour captures the location of the maximum heated region and general characteristic of the temperature distribution, the local temperature distributions around the bottom left part of the exhaust has not been captured accurately. A back projection technique with smoothing and interpolation was applied for the temperature reconstruction [15].

Various reconstruction techniques based on algebraic reconstruction technique (ART), least squares (LSQR) method, and inverse Radon transform have been used for acoustic thermometry [16, 17, 18]. Although refraction effects were not considered in this study, both the LSQR method and multiplicative algebraic reconstruction technique (MART) can be used to integrate the refraction effects due to temperature gradient and flow velocity [16, 18]. The maximum temperature used for circular tomographic simulation is 1200 K with up to 160 K in maximum error without the refraction effect. The maximum error was reduced to maximum of 30 K after accounting for the refraction effect [16]. ART method have shown to estimate temperature up to 340 K with relative errors up to 10% [18].

1.3 Objectives

The present work aims to implementation and development of the acoustic thermometry and tomography technique using simple orthogonal setup. Simplified MART and LSQR methods without considering refraction effects are developed and validated. The bulk mean error (BME) and root-mean-squared percentage error (RMSPE) of the reconstructed temperature were calculated from both tomography techniques to evaluate their abilities of estimating the overall and localized temperatures.

2. Validation of Acoustic Thermometry

2.1 Overview of the Acoustic Technique

As discussed in Section 1.2, the dependence of the speed of sound on temperature of a medium is employed as the fundamental principle for obtaining the line-integrated temperature along the sound path. The relationship between the speed of sound (C) and a gaseous medium temperature is given by,

$$C = \frac{d}{\tau} = \sqrt{\frac{\gamma RT}{M}} \tag{2.1}$$

where d is distance of an acoustic ray path though the medium, τ is the time-of-flight (TOF) of the acoustic wave, γ is specific heat ratio of the medium, R is the universal gas constant, and T and M are the static temperature and the molecular weight of the medium, respectively. The change in the specific heat ratio and gas constant of air is assumed to be negligible due to insignificant effect of the temperature compared with other parameters.

The TOF is an integrated value of along the acoustic ray path which is defined as,

$$\tau = \int \frac{ds}{\sqrt{\gamma RT(s)}} \tag{2.2}$$

where ds is the spatial differential and temperature is a function of space.

2.2 Experiment Setup

Details of the experimental setup utilized for data acquisition are included in the following sections. Section 2.2.1 explains the test conducted for validating an acoustic thermometry technique at room temperature, and Section 2.2.2 details the test setup for heated air temperature measurement.

2.2.1 Acoustic Thermometry Validation Test at Ambient Temperature Condition

To apply the existing acoustic thermometry technique that was mentioned in Section 1.2., the ambient temperature measurement test was conducted using one transmitter and two microphones as shown in Figure 2.1. The first microphone (mic 1) was located before the heated region to obtain raw transmitted signals while the second microphone (mic 2) was placed after the heated region to acquire disturbed acoustic signals. Obtained signals from microphones were used for TOF calculation.

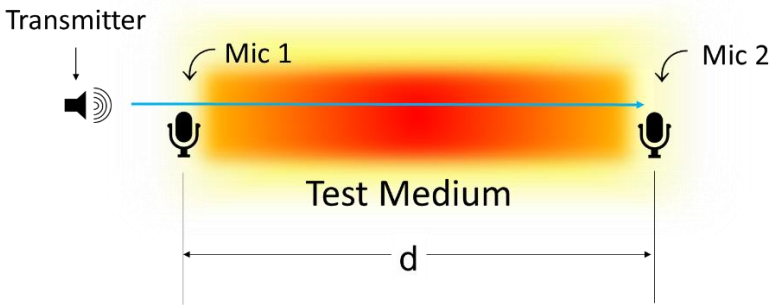

Figure 2.1. Acoustic thermometry validation test setup diagram

The primary equipment used are a 4.8 V input spark gap generator (acoustic pulse transmitting source) and two 6.35 mm free-field PCB microphones (receivers). The spark gap generator has two leads that discharge when the voltage difference of capacitors in series exceeds the dielectric strength of the air, producing an acoustic pulse. An input voltage of 4.5 V was supplied by a 12 V DC generator. The input voltage was set at a slightly lower value than the nominal maximum input voltage to avoid overheating or shortening the lifetime of the spark gap generator. The distance between two microphones measured as 21.9 inches. The signal from the microphone was pre-conditioned by a PCB signal conditioner before being collected into digital files using a NI DAQ system which was controlled by LabVIEW 2014. The data acquisition flow chart is shown in Figure 2.2.

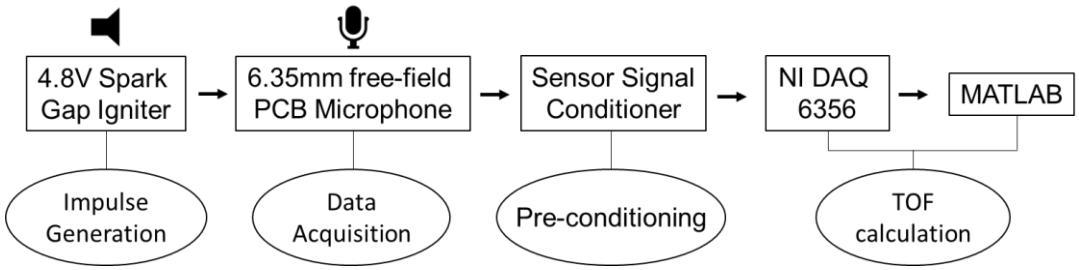

Figure 2.2. Flow chart of the acoustic data acquisition

The acoustic data obtained were then processed to calculate the TOF values of each measurement at ambient temperature condition. The data were sampled at 1.2 MS/s (0.833 MHz) with duration of one second per measurement. Ten measurements were conducted with each measurement containing around 30 acoustic pulses, since the spark gap generator emits approximately 30 pulses per second.

2.2.2 Heated Duct Temperature Measurement

After the validation test data at ambient temperature condition were collected and processed, an experiment at a higher temperature condition was conducted. The compressed air from facility air compressors was supplied into the air hose as shown in Figure 2.3. The air hose was connected with a quick-connect pipe coupling, which connects to an 8 kW Sureheat® Jet inline heater from Sylvania. The compressed air heated by the inline heater was then split by a T-shaped pipe fitting, ultimately merging together into each side of the 3.25 in x 10 in rectangular stainless steel duct through pipes.

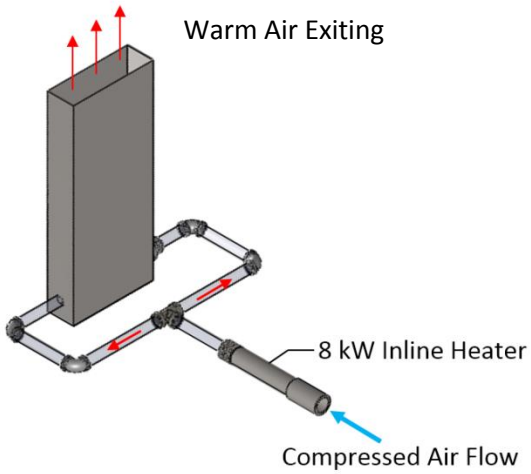

Figure 2.3. The air flow direction from the inline heater to the duct exit

The stainless steel pipes and the rectangular duct were insulated using fiberglass to minimize the heat loss. One pound of steel wool was inserted into the duct to uniformly distribute the heated air exiting through the duct. The velocities of the exiting air were maintained at less than 1 m/s, as measured by a hot wire anemometer. Since the velocities were insignificant compared to speed of sound, the effect of the velocity on sound wave propagation was assumed to be negligible. A straight acoustic travel path without refraction from the air velocity or temperature gradient was assumed in this study.

The transmitter and microphones were setup at the opening of the rectangular duct, as seen in Figure 2.4. The dimension of the duct opening was 3.25 inches by 10 inches. The first microphone (mic 1) was placed before the heated region to obtain transmitter signals and slightly shifted from the centerline to reduce acoustic scattering effects. The transmitter and second microphone (mic 2) were mounted to transmit and receive the acoustic pulse after it had passed through the heated region along the centerline of the duct.

Figure 2.4. View of the bench-top experiment

The measurement plane was shifted one inch in the flow direction from the duct opening to prevent acoustic scattering from the duct. The setup was placed in a lab where walls or reflective surfaces were at least 8 feet away from the transmitter to improve SNR of the obtained data.

For a validation of the technique, a K-type sheathed thermocouple from Omega was placed on the 80/20 structure parallel to the duct centerline. Due to scattering of the signal from the thermocouple, the thermocouple temperature measurement was conducted after the acoustic measurement. The tip of the thermocouple was aligned with the acoustic ray path and was manually traversed to measure temperature along the line. The traverse increment was 0.25 inches, as seen in Figure 2.5, and the duration of each measurement was approximately two minutes to reduce variability from duct exit turbulence by time-averaging. The temperatures were ambient when the measurements were one inch away from the flow, so only 12 inches of thermocouple measurement was conducted.

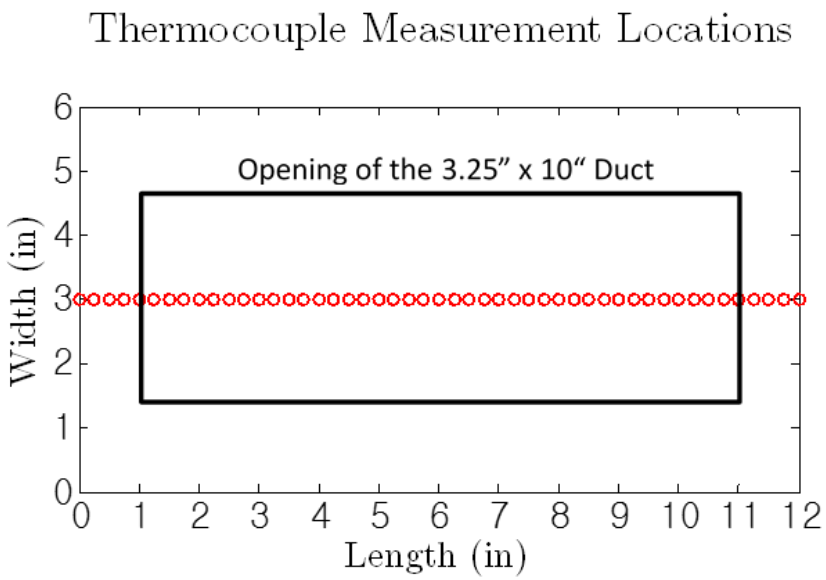

Figure 2.5. Measurement locations of the K-type thermocouple

Another K-type thermocouple was permanently mounted inside of the duct to monitor the temperature of the heated inlet air. The maximum temperature of the air measured by the monitoring thermocouple inside the duct was approximately 500 °F. During a test, both acoustic and thermocouple temperature measurement were conducted only when the monitoring temperature reached the steady-state with the temperature fluctuating less than 20 °F. The monitored temperature ensured that the temperature condition remained consistent for both acoustic and the thermocouple measurement.

2.3 Acoustic TOF Calculation

As mentioned in Section 2.1, the speed of sound travelling through the medium is defined by equation 2.1. The distance between the two microphones – the acoustic wave travelled distance – was physically measured during the setup. The TOF estimates, however, were obtained using the acoustic data, such as in the example in Figure 2.6.

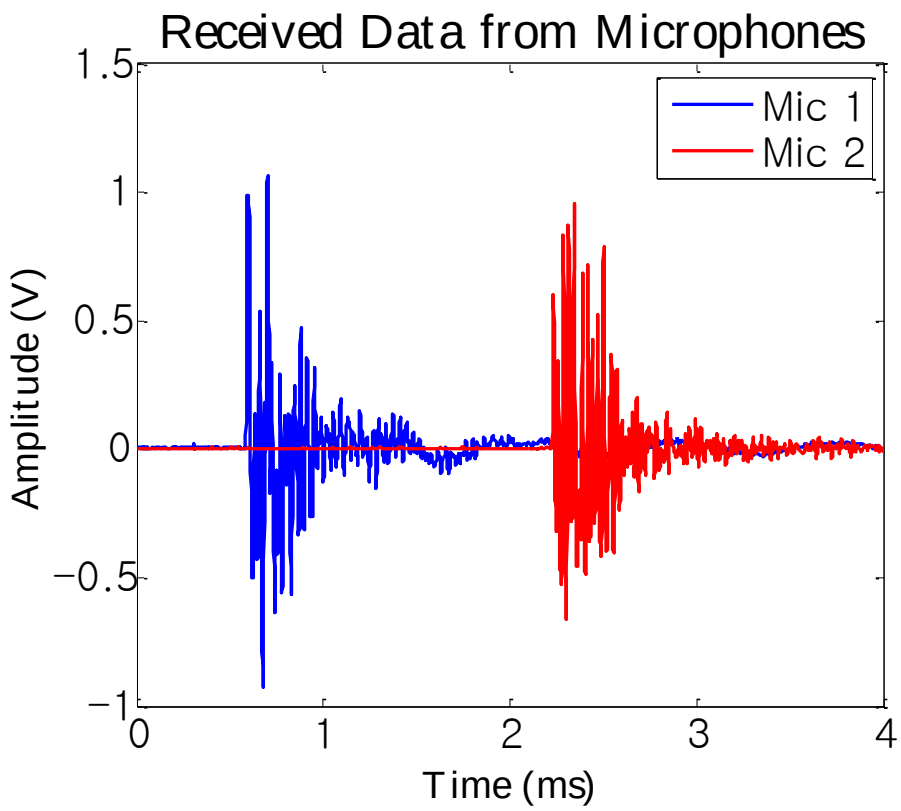

Figure 2.6. Acoustic impulse data from microphones at heated condition

The signals are pre-conditioned through a sensor signal conditioner 482C series by PCB Piezotronics and filtered using low and high bypass filter to reduce the ambient noise and flow noise from the duct. The acoustic pulse has a broad frequency band, complicating elimination

of the noise with filtering. As shown in Figure 2.6, the signal from the second microphone has been slightly distorted and reduced, but the envelopes of both acoustic pulse signals are similar. Without any noise influence, a direct TOF calculation between the signals can be found by obtaining the maximum amplitudes and calculating the delay in the time domain. However, this direct maximum comparison method causes error when the signal is distorted. To ensure accuracy of calculation, the delay between the received signals is computed by using a cross-correlation algorithm.

The cross-correlation algorithm has been used for ultrasonic distance measurement with known gaseous medium properties [19]. The method determines the time delay between a transmitted and reflected signal, such as acoustic signals measured from two microphones. The spark gap generator emits around 33 pulses during one measurement, as shown in Figure 2.7. During the cross-correlation process, the entire measurement signal from the first microphone was correlated with the signal from the second microphone to improve the accuracy at low SNR [4].

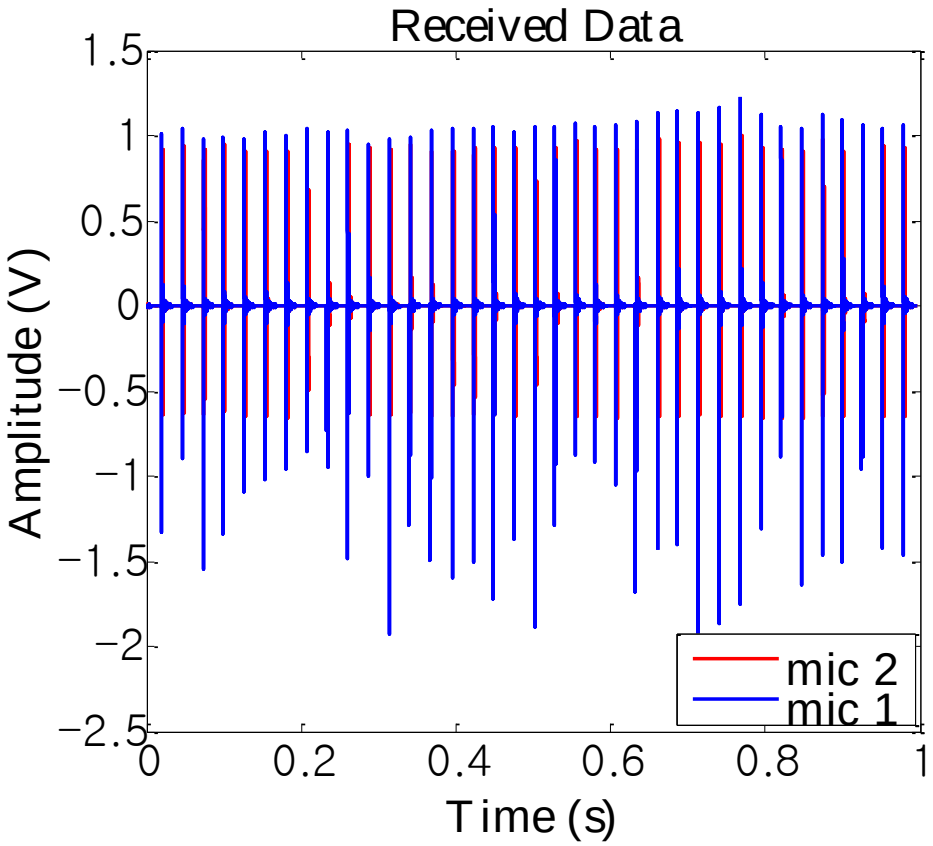

Figure 2.7. Filtered acoustic signal of one second measurement

The cross-correlation coefficients of the acoustic signals calculated from the algorithm indicates the lag at which the signals are most correlated, as seen in Figure 2.8.

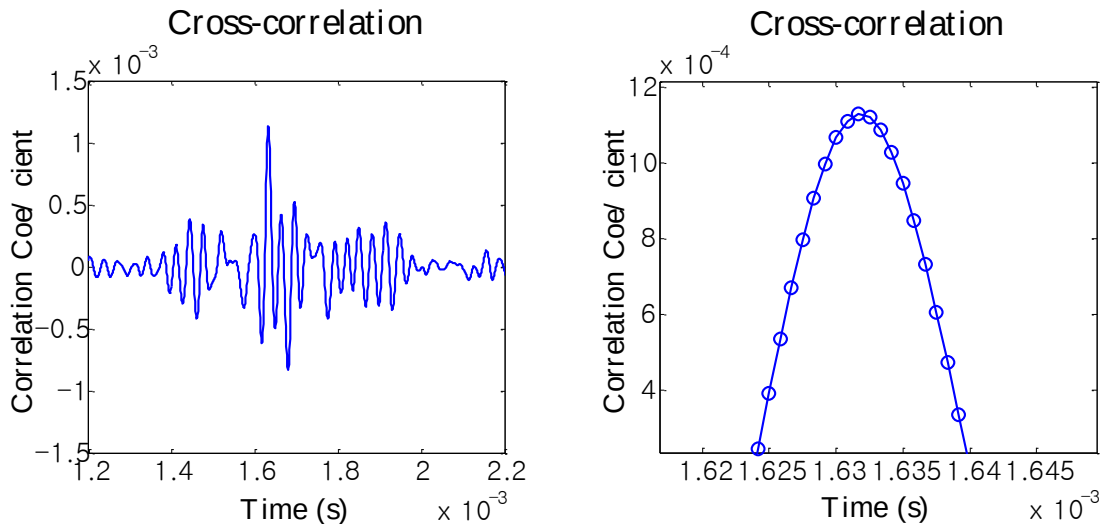

Figure 2.8. Coefficient from the cross-correlation algorithm

The location of the maximum coefficient indicates the lag counts between the two signals. The calculated lag counts were then divided by the sampling frequency to output the estimated TOF of the measurement. With the sampling rate of 0.833 MHz, the resolution of the lag count was found as 0.833 micro-seconds (μs).

2.4 Test Results

The first section discusses the ambient test setup results and the distance calibration process while the second section is focused on the validation of the heated air temperature measurement using acoustic thermometry which is compared with thermocouple-measured temperature data.

2.4.1 Distance Calibration at Ambient Condition

Using the calculated acoustic TOF and measured distance, the speed of sound travelling through the ambient air is obtained. The room temperature measured using acoustic thermometry and a K-type thermocouple showed consistent biased error, and it was concluded that the distance measured by a tape measure was inaccurate due to the difficulty of determining the location of the diaphragm of each microphone inside the microphone cap. Therefore, the room temperature measured by the thermocouple was used to calibrate the distance between transmitter and the microphones. Using equation 2.1, with known temperature and time delays, the distance can be calculated. The calibration of the distance was crucial to determine the

accurate TOF values [19]. The initial distances from the transmitter to the first and second microphone measured by a tape measure were 5.4 inches and 27.3 inches, respectively, and the calibration corrected the distances as 5.5 inches and 27.6 inches. The calibrated distances were used for the heated duct test.

2.4.2 Heated Duct Test Results

With the mounted equipment untouched, the calibrated distances from the ambient temperature measurement were also utilized for calculating the speed of sound for heated air test. To compare the acoustic and thermocouple-measured temperatures within the heated region, the time delays travelling within heated sections were to be calculated. With known lengths of the heated region and ambient region along the acoustic ray path, the Equation 2.2 can be written as,

$$\tau_{total} = \int \frac{ds}{\sqrt{\gamma R T_{ambient}}} + \int \frac{ds}{\sqrt{\gamma R T_{heated}}} + \int \frac{ds}{\sqrt{\gamma R T_{ambient}}} \qquad (2.3)$$

with known ambient temperature. Since thermocouple measurements were taken at a uniform increments, the spatial differential becomes a discrete value and,

$$\frac{d_{heated}}{\sqrt{\gamma R T_{Heated}}} = \tau_{\text{total}} - \frac{2 * d_{ambient}}{\sqrt{\gamma R T_{ambient}}} \qquad (2.4)$$

which can be expressed as,

$$\therefore T_{Heated\ Uniform} = \left(\frac{d_{heated}}{\tau_{\text{total}} - \frac{2 d_{ambient}}{\sqrt{\gamma R T_{ambient}}}} \right)^2 * \frac{1}{\gamma R} \qquad (2.5)$$

The thermocouple measurement shown in figure 2.9 indicates that temperatures outside of the measurement length, 12 inches, are at ambient condition. Therefore, the distance of heated region for comparing acoustic and thermocouple measurement was set as 12 inches, and the length of ambient condition region out of the total length, 22.1 inches, was calculated as 10.1 inches.

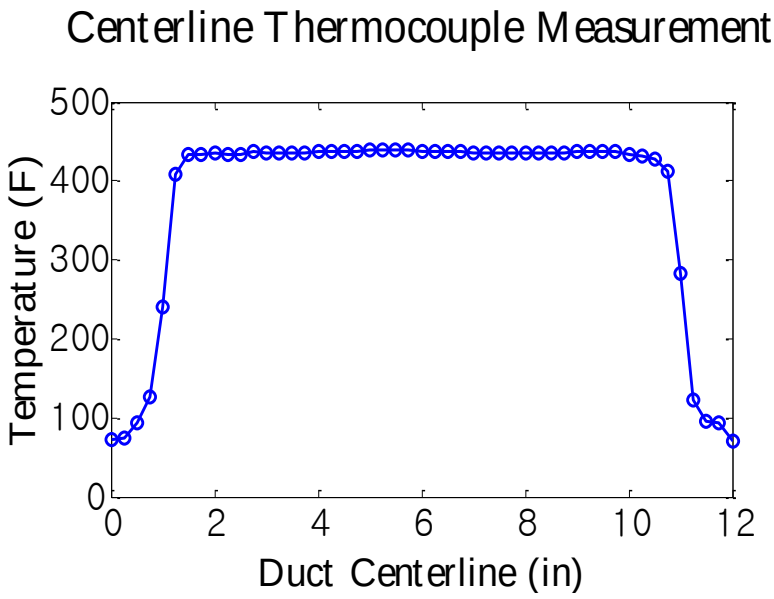

Figure 2.9. Duct centerline temperature distribution of the exiting heated air

The temperatures obtained from the thermocouple were integrated using Equation 2.2 to calculate the uniform temperature within the heated region. The uniform heated temperature obtained from acoustic measurement and the thermocouple measurements are shown in Table 2.1.

Table 2.1. The acoustic heated temperature result.

Thermocouple (°F)	Acoustic (°F)	Absolute Error (°F)	Relative Error (%)	RMSE (°F)
361	358	3	0.3	1.25

The root-mean-square error (RMSE) was calculated using,

$$RMSE = \sqrt{\frac{\sum\left(T_{Acoustic} - T_{Thermocouple}\right)^2}{n}} \tag{2.6}$$

where n represents the number of measurements. The acoustic thermometry measured the temperature within the 1.3 °F root-mean-square error, or 0.3 % relative error calculated in Rankine, compared with the thermocouple-measured temperature data. The uncertainty of the measurement is discussed in detail in Section 4.

3. Heated Duct Temperature Contour Reconstruction

3.1 Experimental Data Acquisition

While single line-of-sight acoustic thermometry measures the integrated temperature along a path, the localized temperature distribution along the path cannot be obtained directly. Because the long-term goal of this research is an instantaneous measurement of jet engine thrust, multiple acoustic ray projection paths and reconstruction techniques are essential for spatially determining the non-uniform temperature contour. With a limited amount of equipment (only two microphones) the construction of a circular arrangement of acoustic ray paths was unfeasible. Therefore, a rectangular arrangement of traversing two microphones with orthogonal ray projections was set up to apply fundamental reconstruction algorithms.

3.1.1 Experimental Setup for Multiple Ray Projections

The temperature distribution of a 2D cross-sectional region coplanar with the opening of the rectangular stainless duct used for the validation test was utilized. The temperature data measured by acoustical thermometry and by K-type thermocouple were collected separately, using an experimental setup shown in Figure 3.1.

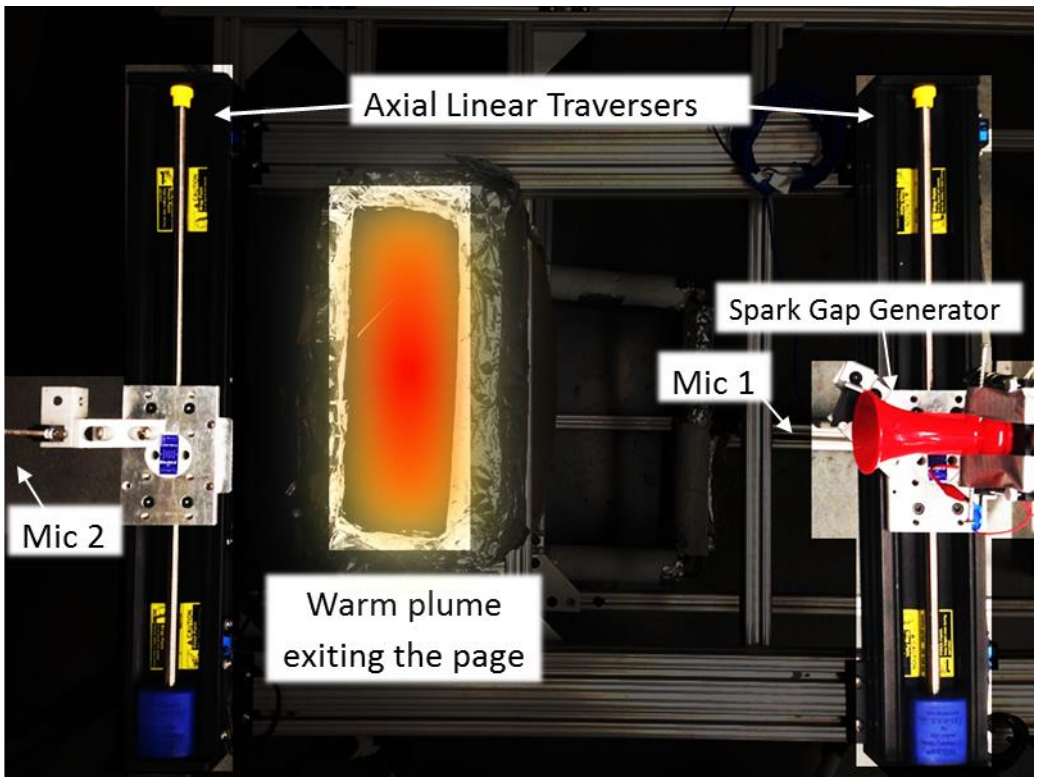

Figure 3.1. Experimental setup for the multiple acoustic ray projections

Two Velmex traverses mounted in parallel were controlled by Cosmos 3.1.6 software. The spark gap generator and the first microphone were mounted on one traverse (RHS) while the second microphone was mounted on the other traverse (LHS). When measurement with the initial projection orientation was finished, the position of the traverses was manually rotated 90°. The total number of acoustic paths for each orientation was 31, and the spacing between each path was set at 0.5 inches, resulting in a 15 inch travel distance. The microphone diaphragm diameter is 0.25 inches, and 0.5 inch spacing increments ensure distinct TOF measurements for each paths. A grid of two orthogonal projections of acoustic rays are shown in Figure 3.2 below. Each line represents an acoustic ray path, creating a 31 by 31 grid. Acoustic and thermocouple measurements were conducted along with the entire span of y-axis to obtain the integrated temperatures of heated region. The width of heated region along the x-axis were relatively narrower and ambient temperature were measured by acoustic and several thermocouples from 0 to 6 inches and 13 to 15 inches of x-axis. Those ambient areas measured by acoustics along the x-axis were assigned with ambient temperatures to reduce the thermocouple measurement time.

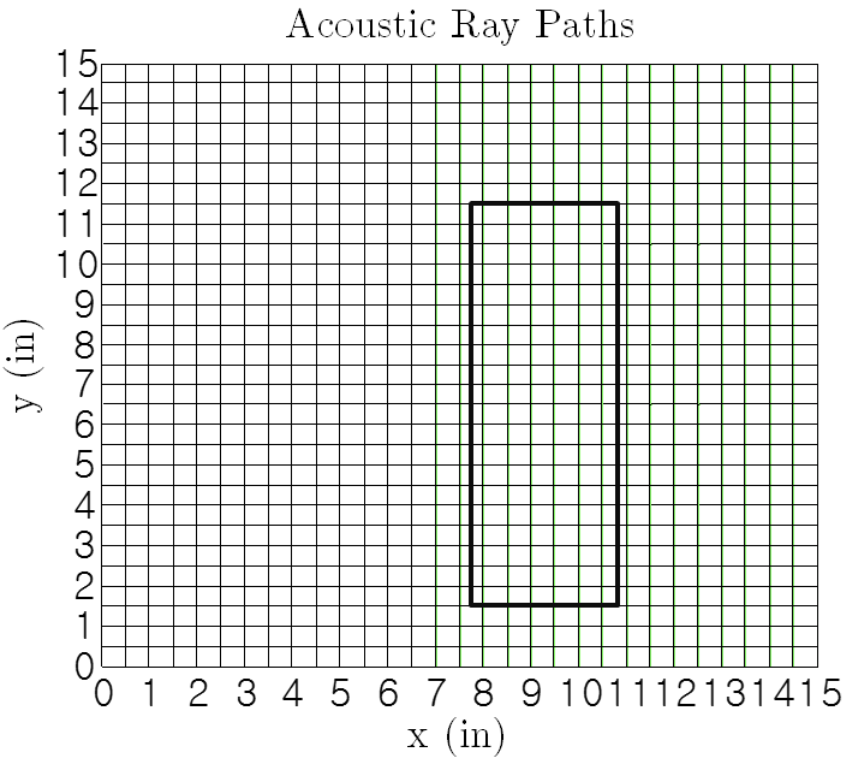

Figure 3.2. Map of acoustic ray paths and location of the rectangular duct

To validate the acoustic temperature measurement, K-type thermocouples were used to measure temperatures at each intersection of horizontal and vertical acoustic lines of sight in

Figure 3.2. Due to the slight temperature fluctuations from turbulence and unsteady flow, the temperature was measured for two minutes and averaged. The location of the 3.25 inch by 10 inch rectangular duct exit is shown in figure 3.2.

3.1.2 Distance Correction

Although the parallel mounting of the traverses was ensured using a tape measure, it was difficult to perfectly align the traverses. As the transmitter and microphones traversed, the TOF values at all traversing locations were collected. The K-thermocouple measured an ambient temperature of 75 °F. Applying the same distance calibration procedure used in Section 2.4.1, ten acoustic measurements at each location were conducted and averaged calibrated distances were calculated. The calibrated distances for the acoustic ray projections are shown in Figure 3.3.

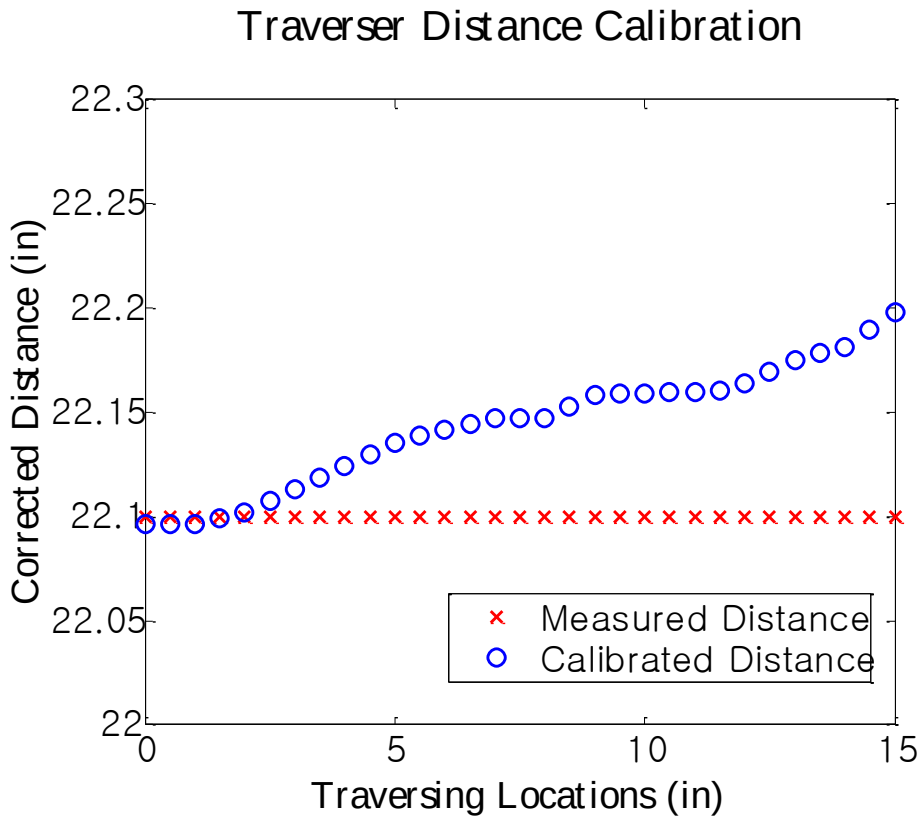

Figure 3.3. Calibrated distance between the microphones

The acoustic ray travel distances became slightly greater as traverses moved. Calibration of the distance eliminated the biased error caused by assuming constant distance for the projections. The calibrated distances were used for obtaining TOFs from tomographic reconstruction techniques.

3.1.3 K-type Thermocouple Temperature Distribution Measurement

As shown in Figure 3.2, the thermocouple-measured temperatures were obtained at each intersection of the acoustic ray projections. A K-type sheathed thermocouple with 1/16 inch diameter was used for measurement. One Velmex traverse mounted perpendicularly on the other traverse enabled control of the thermocouple in horizontal and vertical positions on the temperature measurement plane. As the thermocouple traversed through each location, several minutes were allowed to compensate for the response time. After the temperature fluctuation due to the unsteadiness of the facility was within a 20°F range, measurements were conducted for two minutes at each location and time-averaged. The resulting temperature contour of the duct exit is shown in Figure 3.4.

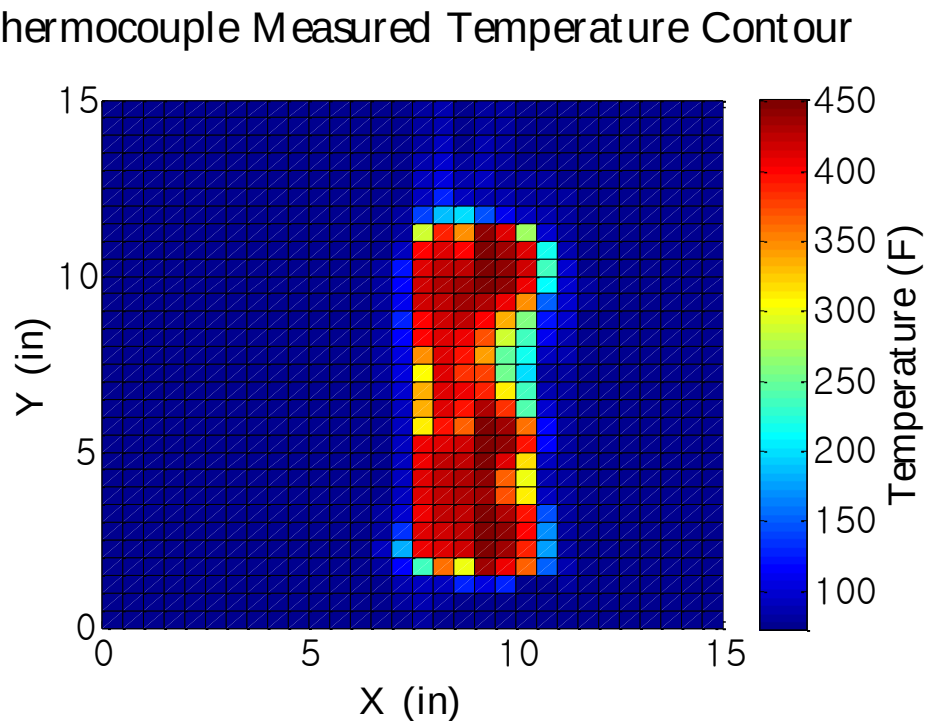

Figure 3.4. Grid map of temperature contour

The contour in Figure 3.4 indicates that lower temperature air is exiting through the middle part of the duct rather than through the top and bottom corners of the duct (region between 9 to 10.5 inches in x-direction and 6 to 8 inches in y-direction). After the acoustic thermometry validation experiment in Section 2, more stainless steel wool was inserted into the duct for better mixing of the heated air. However, uneven distribution of the wool inserted by hand caused a non-uniform temperature distribution. As a result, the temperature

distribution shown in Figure 2.9 differs from the temperature distribution in this section. Despite the unexpected thermocouple results, the obtained temperature contour was studied by developing tomographic reconstructions. The challenge of developing tomographic reconstructions for a non-uniform temperature distribution was important since engine exhaust temperature distributions are not likely to be uniform in real world applications.

3.1.4 TOF from Acoustic Thermometry and K-type Thermocouple

With calibrated distances from Section 3.1.2, the acoustic TOF values were obtained using cross-correlation. The temporally integrated TOF values from the thermocouple-measured temperature distribution were calculated using Equation 2.2. Since the measurement increment was defined as 0.5 inch, the spatial differential becomes a discrete value as shown in Equation 2.3.

The acoustically measured TOF and integrated TOF from thermocouples for both projection angles are shown in Figure 3.5.

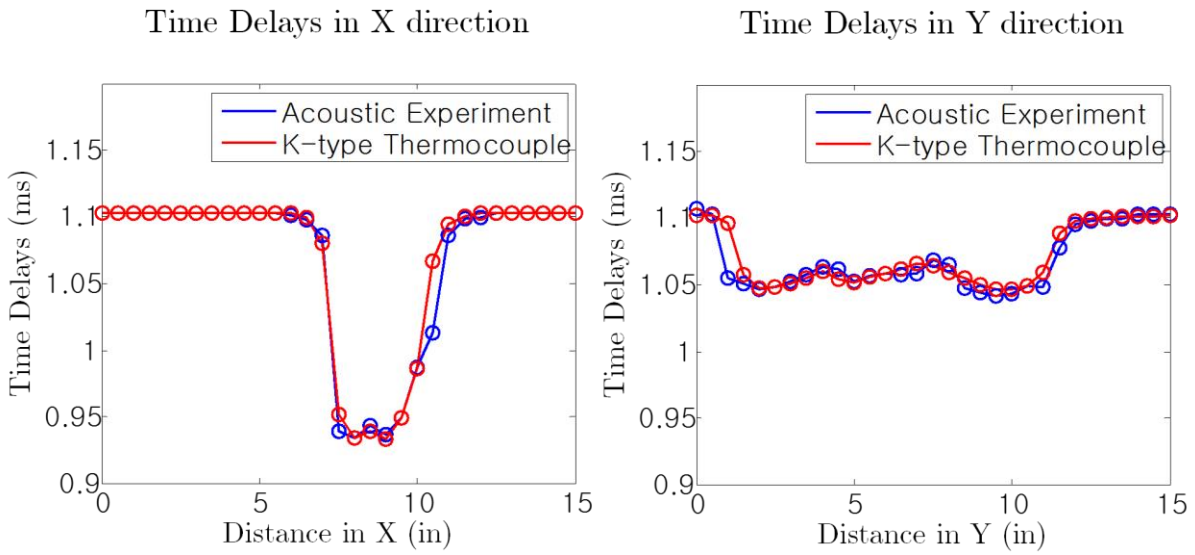

Figure 3.5. TOF values from acoustic and thermocouple measurement

The discrepancies of the TOF between the acoustic and thermocouple measurement are largest where the ray paths travelled near the edges of the duct. The refraction caused by temperature gradient causes the acoustic ray path to curve. The curved path results in inaccuracy of the TOF calculation since the straight distance between microphones is used for calculation. For the tomographic algorithm, the refraction effect was not integrated into equations. Although the integration of refraction effect is not significant (0.15% improvement) for an integrated TOF values at a low temperature, refraction effect integrated reconstruction

algorithms will be developed in the future for the higher temperature conditions since local temperature reconstruction error can be improved by 13% [14, 16].

The reduced TOF values seen in Figure 3.5 indicate the rays are travelling through heated areas. Knowing the ambient condition temperature, the dimensions of the heated area are estimated by analyzing the measured TOF values that are less than the value from ambient condition. Even if the ambient condition temperature data is not available, the dimension of the heated area can be estimated by observing the slope changes in the time delays from the projections that are greater than the heated section. The information from two orthogonal projections is sufficient to estimate the dimension of the heated section since rectangular shape is assumed. For a circular heated area, either the assumption of symmetry or additional projection at different angles will be required. For this experiment, the estimated dimension of the heated section was 3.25 inches by 10 inches, matching the dimension of the rectangular duct exit.

3.2 Development of Tomographic Reconstruction Algorithms

The following sections describe the tomographic reconstruction algorithms that were developed for the rectangular heated region. The least squares method and multiplicative algebraic reconstruction technique are explained in depth.

3.2.1 Least squares method (LSQR Method)

As seen in Figure 3.2, the number of acoustic ray intersections is greater than the number of the rays, and using a system of linear equations to calculate the temperature at intersections becomes an underdetermined problem. Since a direct method cannot be used, unknown temperatures at each intersection were estimated using the least squares method. In principle, the least squares method compares the simulated TOF values with actual TOF values from the experiment, estimating the simulated temperature fields resulting the least squared errors.

The unknown heated area dimension is estimated using the TOF information and the area is divided into multiple estimated sections where the guessed temperature values are assigned for each iteration. During the iteration, with every combinations of iterative temperatures are assigned, temporally integrated TOF values are generated using Equation 2.2. The generated TOF values from iterations are then compared with the actual measured TOF

values to determine which combination of temperatures assigned into estimated sections is most accurate. The error between the measured and generated TOF values are defined as

$$\phi = \sum_{i=1}^{M} \sum_{j=1}^{N} \left(\tau_{generated}^{i,j} - \tau_{measured}^{i,j}\right)^2 \tag{3.1}$$

where the ϕ is the squared error to be minimized and M and N represents the number of acoustic rays projections at each orthogonal angle. The iterative process repeats until least squared error values (ϕ) is found, determining the optimal estimated temperature distributions.

Before implementing the least squares method with measured experimental acoustic data for reconstructing the heated duct temperature distribution, simulations with simple generated temperature fields were used for validation of the least squares method algorithm. The uniform generated temperature field at 600 °F with similar dimension as the rectangular duct was used as seen in figure 3.6.

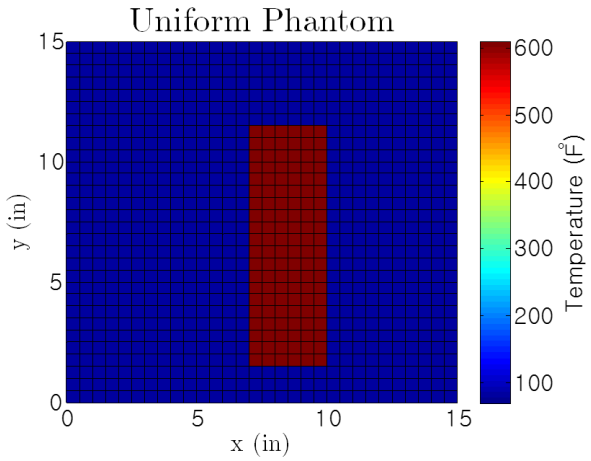

Figure 3.6. Phantom temperature contour with uniform temperature

Also, simulation using inhomogeneous temperature field were conducted to further validate the reconstruction method. The phantom contour bounded by duct dimensions with 3, 6, and 9 division sections are generated as shown in Figure 3.6.

Table 3.1. Phantom generated heated sections values for 3, 6, and 9 temperature sections

Temperatures assigned for each sections (°F)					
3 section	6 section		9 section		
350	370	350	405	420	330
405	315	305	380	380	205
333	370	333	400	420	300

The phantom contour with duct dimension with 3, 6, and 9 division sections are generated as shown in Figure 3.6.

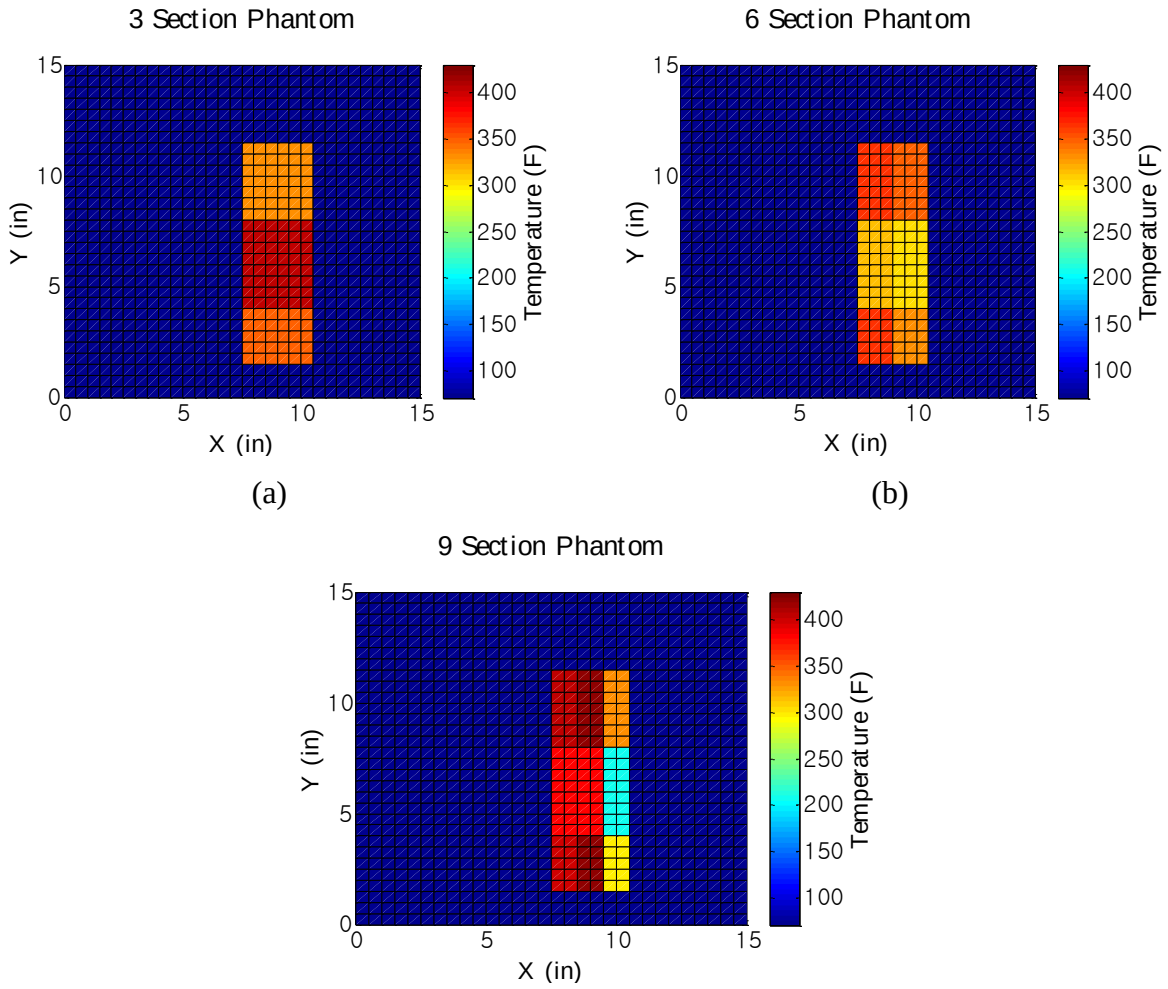

(a) (b)

(c)

Figure 3.7. Phantom temperature contour with 3, 6, and 9 sections

For the phantom simulations, the temporally integrated TOF values from the phantom temperature contours were assigned as the true measured values instead of experimental data. For each case, the set of iterating temperature values was assigned for each individual section.

Since the least squares method is an iterative process, the computation time of the temporal integration for every iteration increased in magnitude with increasing number of estimation sections [16]. With grid configuration shown in Figure 3.2, total of 120 sections can be used for the LSQ method. However, bulk estimation sections were assigned to reduce the computational cost. The estimations were mainly assigned as 3, 6, and 9 division sections.

Also, increasing the range of the iterating temperature increases the computational time since the iterating residual increases. Determining a reasonable range of the iterative

temperature was necessary since iterating temperature from room temperature to the guessed maximum temperature is impractical. Using the Equation 2.2 and the dimension constraints calculated from the TOF, the uniform temperatures within the heated area were calculated for every ray path from both projections. For each divided section, the uniform temperature within the section was averaged and set as the initial guess.

The range of the temperature is defined by setting the minimum and the maximum of the range and also the increments of the temperature value in between the minimum and maximum values. When simulating more than six sections, the computational time for each iteration (i) increased geometrically [16]. Once the minimum (a_i) and maximum (b_i) values for the temperature range is set, a variant of the bisection root-finding method is applicable. First, the midpoint (m_i) of the interval is calculated taking the average of $[a_i, b_i]$. Then least squares error is calculated for all three temperatures, $\langle E_a, E_b, E_m \rangle = LSQ\langle a_i, b_i, m_i \rangle$. If error is minimized at the lower bound, that is, $\min(\langle E_a, E_b, E_m \rangle) = E_a$, then the midpoint becomes the new upper bound $(b_{i+1} = m_i)$ and the next iteration begins. A similar approach is used if error is minimized at the upper bound, b_i. However, if error is minimized at the mid-point, m_i, the temperature range is cut in half by moving the upper and lower bounds towards the midpoint:

$$a_{i+1} = a_i + \frac{b_i - a_i}{4}$$

$$b_{i+1} = b_i - \frac{b_i - a_i}{4} \tag{3.2}$$

$$m_{i+1} = m_i$$

Stopping conditions for the optimization are a maximum number of iterations and a minimum error tolerance. For LSQR methods, estimation converged after 20 iterations. The optimization iterative process was implemented to the 3, 6, and 9 section phantom least squares method simulations. The temperatures assigned for the phantom sections were the averaged values of the thermocouple data at the same location.

3.2.2 Simplified Multiplicative Algebraic Reconstruction Technique (SMART)

The traditional MART utilizes multiple projections at various angles which enables more accurate reconstruction. Having two orthogonal projections, a simplified MART approach was developed.

MART method utilizes the averaged values from each path instead of integrated values. Acoustic thermometry data, however, is in a temporally-integrated form, for which the result differs from the averaging technique when the discretized increments become coarse. For the reconstruction, sufficiently fine grid size was used so that the deviation with integrated and averaged values is below 0.01%.

Unlike LSQR method, SMART sums all the uniform heated temperature values from the projection and averages them. Then the averaged value is used as the initial guess for all of divided estimation sections. The temporally integrated TOF values are calculated from the guessed temperature distribution. Fundamentally, SMART calculates the ratio between TOF from the initial averaged temperature distribution and the experimentally measured data.

The SMART multiplies the coefficients to the initial values, which the process can be simply expressed as,

$$a_j^{k+1} = a_j^k * \left(\frac{\tau_{i_{measured}}}{\langle D_i \cdot a^k \rangle} \right)^{\lambda * D_{ij}} \tag{3.3}$$

where i and j represent the location of the grid cell in row and column, respectively, a is the reciprocal of the speed of sound in each grid cell, D is the point spread matrix, and λ is the relaxation coefficient for the convergence. With two orthogonal projections, the multiplicative correction factor becomes constant after one iteration. In this study, SMART method was used as an analytical method since only two angles were used.

To validate the applied SMART algorithm, the phantom generated temperature distributions shown in Figure 3.6 and 3.7 were used. After the phantom simulation was conducted, the algorithm was applied to the temperature distribution measured by using thermocouples.

3.3 Algorithm Simulation Results

Both LSQR and SMART reconstruction methods were simulated with phantom temperature distributions having 3, 6, and 9 distinct temperatures. The results are discussed in Section 3.3.1. The results of simulating the reconstruction of the temperature distribution measured using thermocouples are shown in Section 3.3.2.

3.3.1 Phantom Generated Simulations

Using both LSQR and SMART method, the uniform temperature contour shown in figure 3.6 was reconstructed to 600°F, validating that both methods can reconstruct accurately if the temperature is uniform. For LSQR methods, 3, 6, and 9 estimation sectioning were applied and successfully reconstructed to the exact phantom temperature on all cases.

With the inhomogeneous phantom temperature contours, the reconstruction techniques began to reveal their limitations on reconstructions. The root-mean-square error between the reconstructed temperature values from the LSQR method and SMART using the phantom generated values is calculated,

$$RMSE = \sqrt{\frac{\sum(T_{Reconstructed} - T_{Phantom\ Generated})^2}{N}} \tag{3.4}$$

where N represents the number of temperature grid points. For all of LSQR method and SMART results, N was set as 120 since the dimension of the heated area was defined as 6 grid blocks by 20 grid blocks.

The root-mean-square error values of both techniques for three different phantom distributions shown in figure 3.7 were calculated. The results are shown in Table 3.2.

Table 3.2. Root-mean-square errors from phantom temperature distribution

RMSE values (°F)	LSQR	SMART
3 Sections	0.34	0.03
6 Sections	6.37	5.06
9 Sections	29.67	20.92

With only two perpendicular projections, the accuracy of reconstruction decreases as the temperature distribution becomes non-uniform and asymmetric. The SMART was more accurate for reconstructing all three different temperature distributions than the LSQR method. However, both method reconstructed a uniform heated temperature field to the exact temperature, and the higher error in LSQR method will be resolved when more estimation sections are applied.

3.3.2 Reconstruction Simulations Using Thermocouple-Measured Data

The following sections discuss the results of reconstruction of temperature distributions measured by thermocouple. Since the thermocouple-measured temperature values are used as a reference to validate the acoustic tomographic reconstruction technique, the accuracy of the techniques was studied by applying the algorithms to thermocouple-measured temperature distribution maps. The simulated acoustic TOFs projected through the temperature distribution were calculated using Equation 2.2 as shown in Figure 3.5. The comparisons of the temperature distribution from the thermocouple data and from the LSQR method are shown in Figure 3.7. Since the LSQR method reconstructs the temperature distribution with 3, 6, or 9 sections, the thermocouple-measured temperature within the corresponding dimension were area-averaged for visual comparison. Reconstructed temperature distribution from the SMART method and the absolute errors between thermocouple data are shown in Figure 3.8. For easier contour comparison, only the data within the heated region is shown. For the root-mean-square error calculation, entire temperature distributions, including the heated regions, were used. The root-mean-square error of temperature reconstruction of both techniques was calculated using Equation 3.4, and is shown in Table 3.3.

(a)

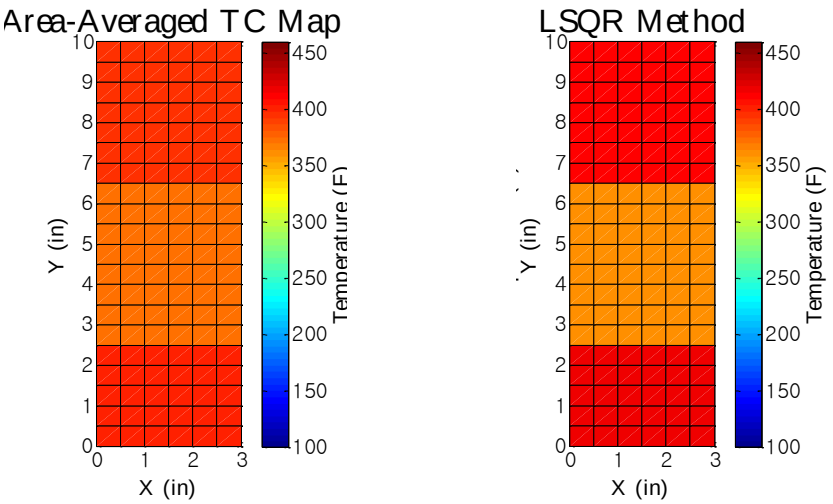

(b)

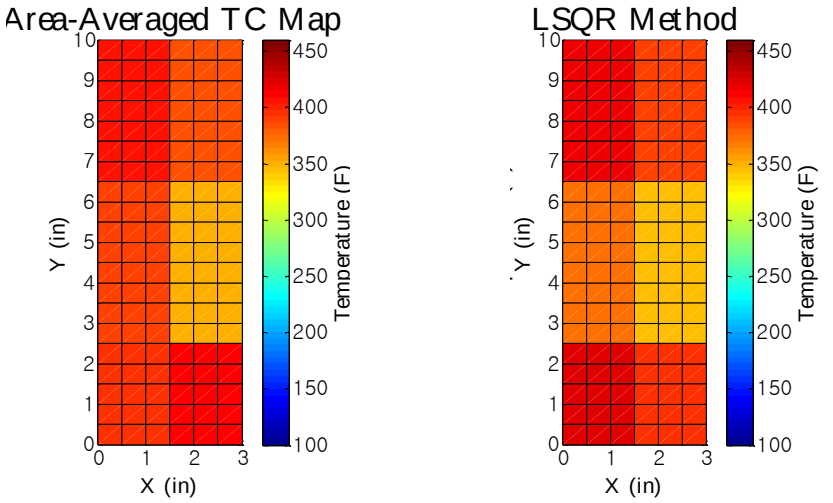

(c)

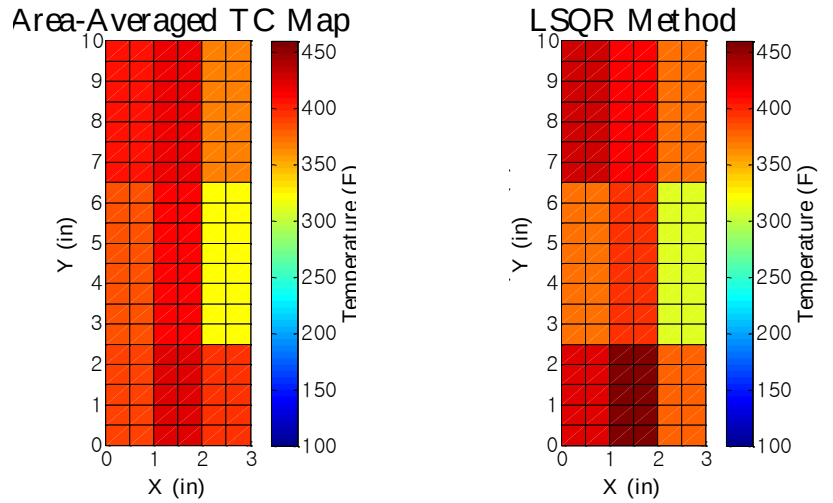

Figure 3.8. Comparison of the contours from the thermocouple measurement and LSQR reconstruction simulation for 3 (a), 6 (b), and 9 (c) sections

(a) (b)

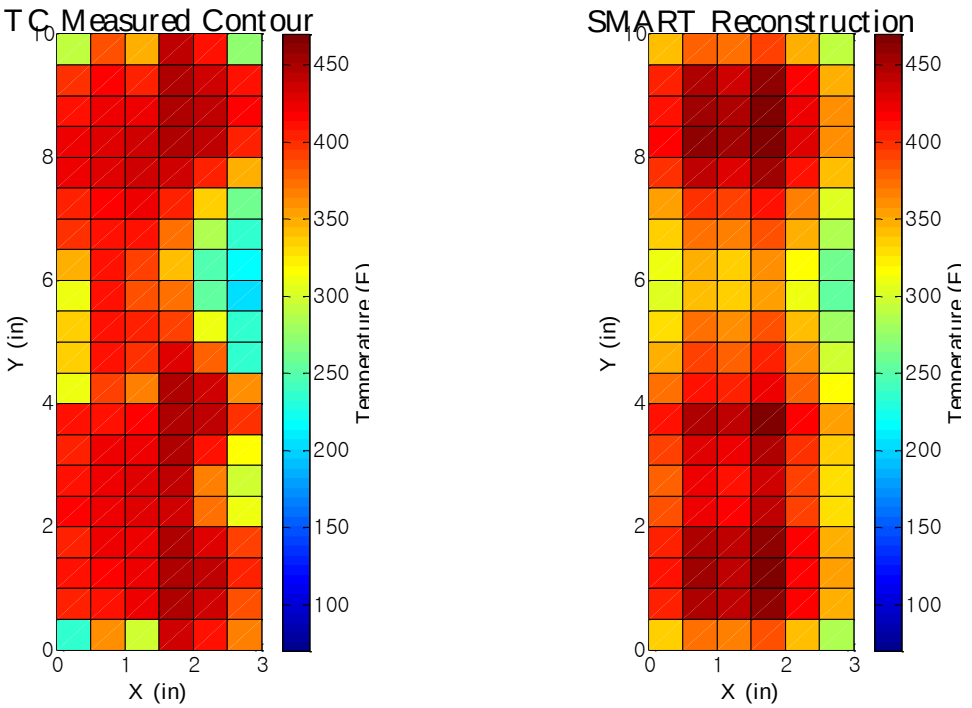

(c)

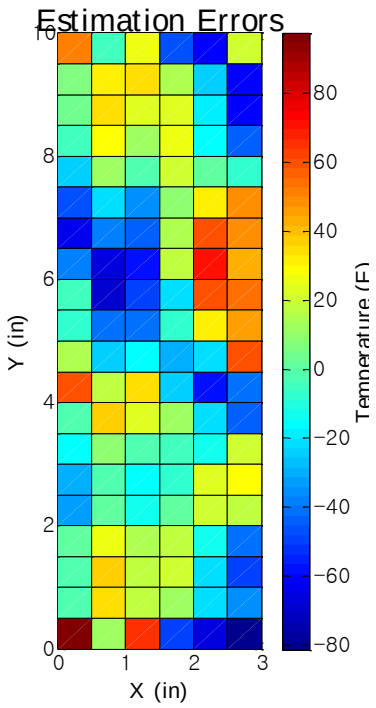

Figure 3.9. Contours from thermocouple measurement (a), reconstructed with SMART simulation (b), and the absolute error calculated (c)

Table 3.3. Absolute RMS errors of reconstruction techniques from the simulation

RMSE of LSQR Method (°F)			RMSE of SMART (°F)
3 section	6 section	9 section	120 section
56.5	55.41	51.5	32.73

Although the root-mean-square error values are high, both tomographic reconstruction techniques have captured the characteristics of the temperature contour. Lower errors of the reconstruction were achieved as number of estimation section increased, giving SMART advantage over LSQR method.

The estimation sections reconstructed by the LSQR method have successfully estimated the hotter and colder regions of the contour. The SMART also recreated resembling contours of the temperature distributions. The non-uniform and asymmetric temperature contour increased the reconstruction error for both tomographic reconstruction techniques, but the overall temperature contours were contained.

3.4 Experimental Reconstruction Results

After the algorithms were validated, the acoustic TOF values from the experiment, shown in Figure 3.5, were implemented to reconstruct temperature distributions. The reconstruction results of LSQR method are shown in Figure 3.9, and the result of the SMART is shown in Figure 3.10. Unlike the results in Section 3.3.2, most values of reconstructed temperature distributions are higher than the thermocouple data for both techniques.

Table 3.4. Absolute RMS errors of reconstruction from experimental data

RMSE of LSQR Method (°F)			RMSE of SMART (°F)
3 section	6 section	9 section	120 section
74.93	69.60	66.74	63.77

The root-mean-square errors, as shown in Table 3.4, are greater than the simulated case. The majority of errors are due to the effect of refraction, as the acoustic TOF values tend to be lower around the heated plume since the ray travels faster through the heated region. The error from refraction can be reduced by 13% when the refraction effect is integrated [16]. The inhomogeneity of the temperature distribution is also a factor of the error. Although the temperature values from thermocouple measurements and acoustic measurements are time-averaged, the fluctuations of the temperature may still have an influence on the accuracy of the measured TOF values.

(a)

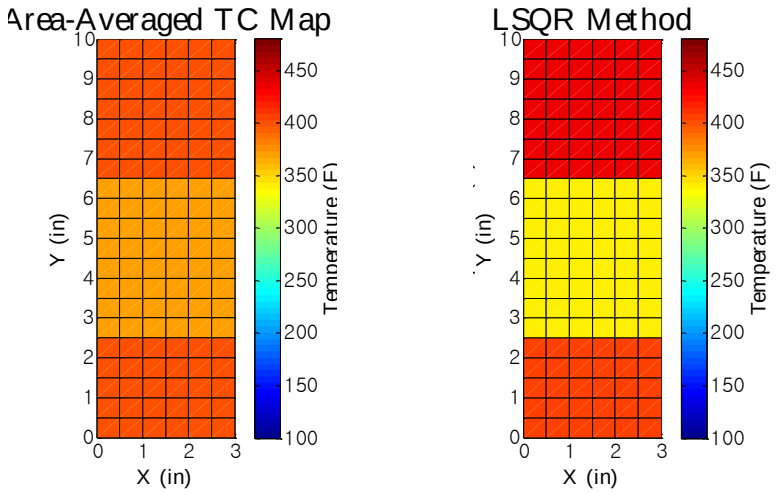

(b)

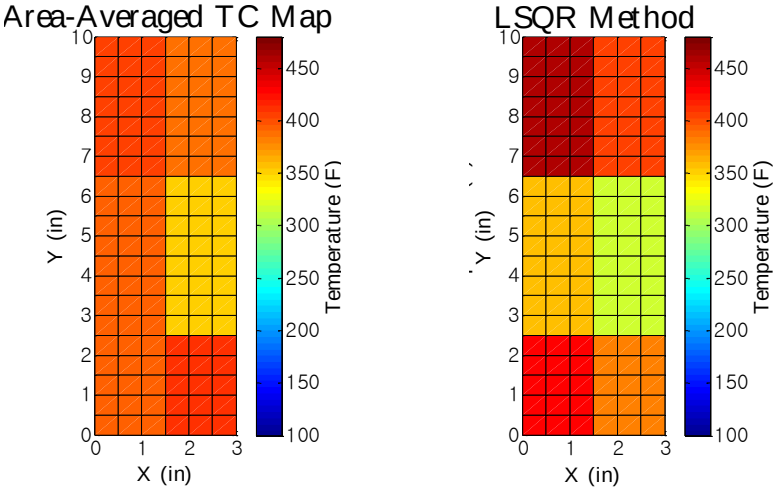

(c)

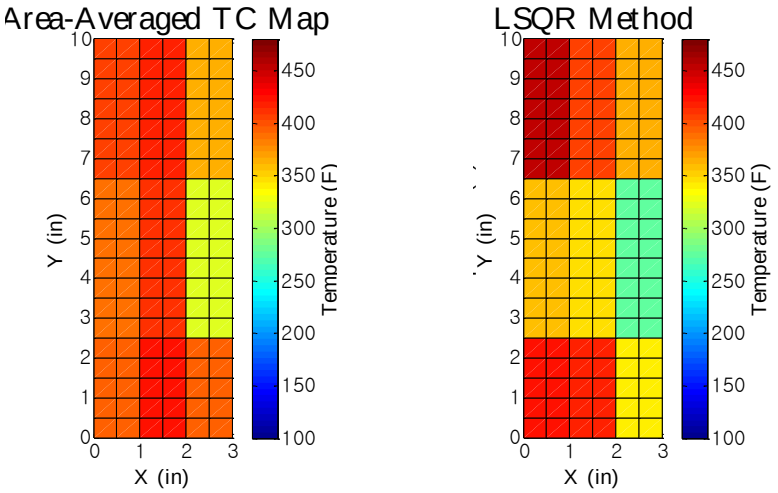

Figure 3.10. Comparison of the contour from the thermocouple measurement and LSQR reconstruction from experimental TOF values for 3 (a), 6 (b), and 9 (c) sections

(a) (b)

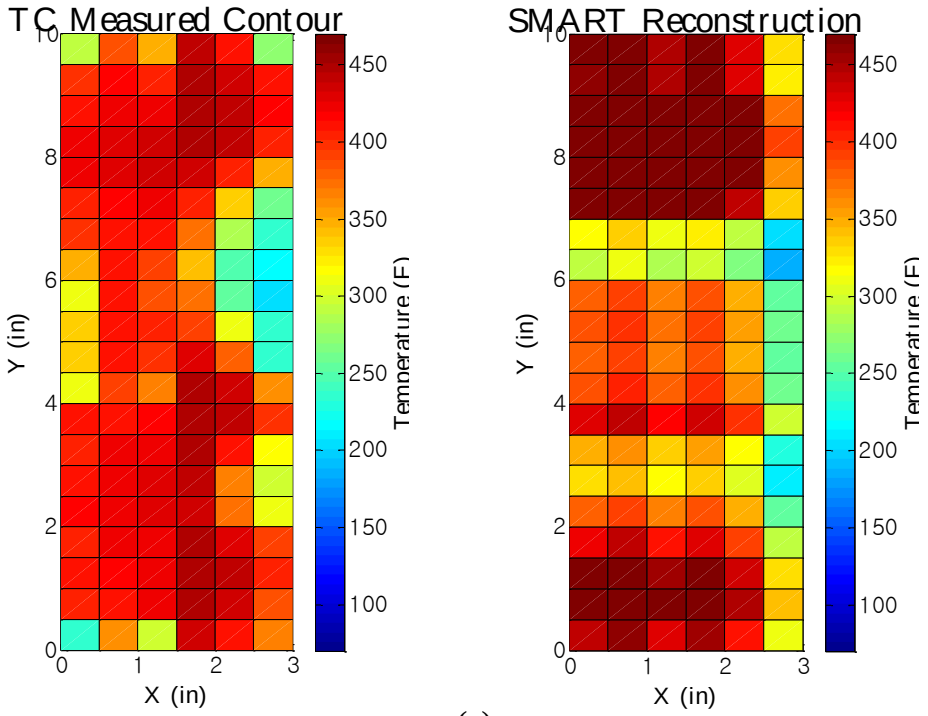

(c)

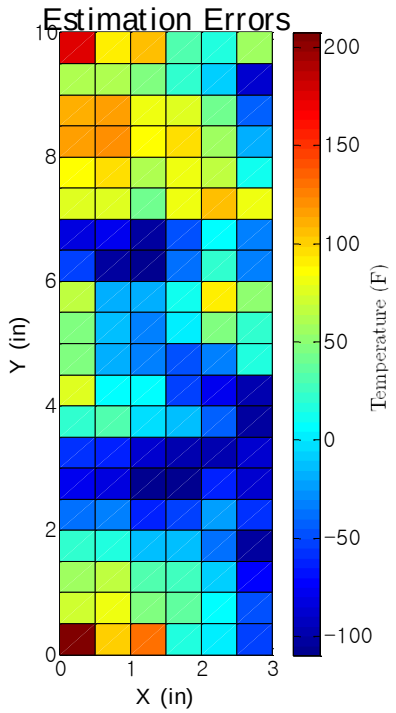

Figure 3.11. Contour from thermocouple measurement (a), reconstruction with SMART using experimental TOF values (b), and the absolute error calculated (c)

4. Uncertainty Analysis

The uncertainty of the acoustic thermometry and theoretical limitations of tomographic reconstruction with two orthogonal projections are discussed in this chapter. Uncertainties from equipment and signal processing are calculated. The fluctuation of the temperature is assumed to be negligible due to time-averaging. The effect from acoustic ray refraction will be investigated in the future.

From the Equation 2.1, the temperature term can be expressed as

$$T = \frac{M}{\gamma R}\left(\frac{d^2}{\tau^2}\right) \tag{3.5}$$

The uncertainty of temperature measurement,

$$U_T = \sqrt{\left(\frac{\partial T}{\partial d} * u_d\right)^2 + \left(\frac{\partial T}{\partial \tau} * u_\tau\right)^2} \tag{3.6}$$

which becomes,

$$\therefore U_T = \sqrt{\left(\frac{2}{kR(\tau)^2} d * u_d\right)^2 + \left(-\frac{2d^2}{kR(\tau)^3} * u_\tau\right)^2} \tag{3.7}$$

where U_T is the absolute uncertainty of the temperature, and u_d and u_t are the uncertainty of the distance and TOF value, respectively.

It is shown that the temperature measurement depend on distance measurement and time delay calculation. Since the distance for acoustic thermometry is calibrated using thermocouple, the u_d term depends on thermocouple accuracy. The Omega K-type thermocouple typically has an error of $\pm$ 2 ℃ at room temperature. The distance absolute error was found to be 0.08 inches or 0.0018 m from the acoustic distance measurement.

The uncertainty in the TOF calculation was determined by the sample frequency of the data, which is 1.2 MS/s. The smallest time steps used for cross-correlation is inverse of the

sampling rate, which is 0.83 microseconds. Using the distance and time delay uncertainties, the absolute uncertainty of the temperature was found as 5.6 °F.

For the tomographic reconstruction limitation analysis, the results of simulated and experimental tomographic reconstructions are compared with bulk mean errors (BME), mean relative errors (MRE) and root-mean-square percentage errors (RMSPE). For LSQR method, only the 9 section case results were used for the calculation.

The bulk mean error was calculated by area-averaging the temperature within the estimated dimension of the heated section and comparing for both thermocouple-measured and reconstructed values [14]. The mean relative error was calculated by normalizing the relative error for each grid point within the heated area, and the root-mean-square percentage error was found by normalizing the bulk mean value of the thermocouple-measured temperature within the heated area. The equations are defined as in [1],

$$MRE = \frac{1}{n}\sum\left(\frac{T_R - T_{TC}}{T_{TC}}\right) * 100\% \qquad (3.8\text{ a})$$

$$RMSPE = \frac{\sqrt{\left(\frac{1}{n}\right)\sum(T_R - T_{TC})^2}}{T_{TC\ Mean}} * 100\% \qquad (3.8\text{ b})$$

where T_R represents the reconstructed temperature, T_{TC} is the thermocouple-measured temperature, n is the total number of temperature grid points, and $T_{TC\ Mean}$ is the area-averaged temperature. The results are shown in Table 4.1. The LSQR method

Table 4.1. Absolute RMS errors of reconstruction from experimental data

	LSQR 9 section		SMART	
	Simulation	Experiment	Simulation	Experiment
BME	0.8 %	5.09 %	0.3 %	1.3 %
MRE	12.2 %	21.2 %	9.9 %	17.9 %
RMSPE	14.8 %	20.7 %	9.8 %	18.9 %

The errors of LSQR method were similar for both simulation and experiment cases. Since estimation section division of 3, 6, and 9 sections was applied to reduce the computational time, local temperature distributions were difficult to achieve for both simulation and experiment. Also the averaging of the area reduced the difference between the simulation and experimental error. The SMART method performed better in both simulation

and experiment reconstruction since every grid cells were estimated. The error of the estimation increased during experiment reconstruction due to local temperature errors caused by refraction effect.

5. Conclusions

In many engine exhaust temperature measurements, intrusive methods are commonly used. Due to cost and inaccuracy of intrusive methods, a non-intrusive temperature measurement method is desired. In this study, a non-intrusive temperature measurement approach using acoustic properties has been applied for reconstructing temperature distributions.

Acoustic thermometry with a cross-correlation algorithm to determine TOF values of acoustic rays has been developed and utilized to measure the temperature of the heated region with negligible velocity within 0.3% relative error. Although the measurements employed the time-averaging technique, error due to fluctuation observed and can be further improved with longer data collection time.

Tomographic reconstruction algorithms based on LSQR and SMART methods have been developed for a rectangular heated region. Due to the limitation of available equipment, a rectangular arrangement of acoustic ray projections with a traversing mechanism was utilized. The results indicates that two orthogonal projections were sufficient to reconstruct the general characteristic of a non-uniform, asymmetric temperature contour, however, the accuracy of the reconstructed local temperatures can be improved in the future with additional projection angles. In comparison, the SMART has slightly higher accuracy of reconstruction than the LSQR method. The better accuracy of LSQR method is expected to be achieved with increased number of estimation sections in the future.

The algorithms for reconstructing temperature contours using two orthogonal projections have been applied and confirm the capability of reconstructing the contour characteristics. These methods will be further developed for applications using multiple angles of projections and integrating the effect of refraction from the temperature gradient and with significant velocity.

6. References

[1] X. Shen, Q. Xiong, W. Shi, S. Liang, X. Shi and K. Wang, "A New Algorithm for Reconstructing Two-Dimensional Temperature Distribution by Ultrasonic Thermometry," *Mathematical Problems in Engineering,* vol. 2015, pp. 1-10, 2015.

[2] A. Kosugi, I. Ihara and I. Matsuya, ""Accuracy evaluation of surface temperature profiling by a laser ultrasonic method," *Japanese Journal of Applied Physics,* vol. 51, no. 7, 2012.

[3] H. Yamada, A. Kosugi and I. Ihara, ""Noncontact monitoring of surface temperature distribution by laser ultrasound scanning," *Japanese Journal of Applied Physics,* vol. 50, no. 7, 2011.

[4] R. Otero, K. T. Lowe and W. Ng, "Extension of Sonic Anemometry to High Subsonic Mach Number Flows," *Measurement Science and Technology,* (To be submitted).

[5] J. Tyndall, Sound, 3rd ed., New York: Appleton, 1875.

[6] S. G. Schock, "A method for estimating the physical and acoustic properties of the sea bed using chirp sonar data," *IEEE Journal of Oceanic Engineering,* Vols. 29, no. 4., pp. 1220-1217, 2004.

[7] T. Schlegl, B. T, N. M and Z. H, "Combined Capacitive and Ultrasonic Distance Measurement for Automotive Applications," *IEEE sensors journal,* Vols. 11, no. 11, pp. 2636-2642, 2011.

[8] Y. Huang and D. Chen, "Automatic Contouring for Breast Tumors in 2-D Sonography," in *IEEE Engineering in Medicine and Biology*, Shanghai, 2005.

[9] E. V. Ostashev, N. S. Vecherin, D. K. Wilson, A. Ziemann and H. G. Goedecke, "Recent Progress in Acoustic Tomography of the Atmosphere," in *IOP Conference Series: Earth and Environmental Science*, 2008.

[10] H. Yamoaka, A. Kaneko, J. Park, H. Zheng, N. Gohda, T. Takano, X. Zhu and Y. Takasugi, "Coastal Acoustic Tomography System and Its Field Application," *IEEE Journal of Oceanic Engineering,* vol. 27, no. 2, pp. 283-295, 2002.

[11] M. Bramanti, E. A. Salerno, A. Tonazzini, S. Pasini and A. Gray, "An Acoustic Pyrometer System for Tomographic Thermal Imaging in Power Plant Boilers," *Instrumentation and Measurement,* vol. 45, no. 1, pp. 159-167, 1996.

[12] H. Sielschott, "Measurement of Horizontal Flow in A Large Scale Furnace Using Acoustic Vector Tomography," *Flow Measurement and Instrumentation,* vol. 8, pp. 191-197, 1997.

[13] J. Kleppe, J. Sanches and G. Fralick, "The Application of Acoustic Pyrometry to Gas Turbine and Jet Engines," *AIAA,* Vols. 98-3611, 1998.

[14] U. DeSilva, R. H. Bunce and H. Claussen, "Novel Gas Turbine Exhaust Temperature Measurement System," in *Proceedings of ASME Turbo Expo 2013: Turbine Technical Conference and Exposition*, San Antonio, Texas, 2013.

[15] U. Desilva, R. H. Bunce, J. M. Schmitt and H. Claussen, "Gas Turbine Exhaust Temperature Measurement Approach Using Time-Frequency Controlled Sources," 2015.

[16] J. Lu, K. Wakai, S. Takahashi and S. Shimizu, "Acoustic Computer Tomographic Pyrometry for Two-Dimensional Measurement of Gases Taking into Account the Effect of Refraction of Sound Wave Paths," *Measurement Science and Technology,* vol. 11, no. 6, pp. 692-697, 2000.

[17] P. Holstein, A. Raabe, R. Muller, M. Barth, D. Mackenzie and E. Starke, "Acoustic Tomography on the Basis of Travel-Time Measurement," *Measurement Science and Technology,* vol. 15, no. 7, pp. 1420-1428, 2004.

[18] P. Beckord, G. Hofelmann, H. O. Luck and D. Franken, "Temperature and Velocity Flow Fields Measurements using Ultrasonic Computer Tomography," *Heat and Mass Transfer. vol. 33, no. 5,* pp. 395-403, 1998.

[19] S. Hirata, M. K. Kurosawa and T. Katagiri, "Accuracy and Resolution of Ultrasonic Distance Measurement with High-Time-Resolution Cross-Correlation Function Obtained by Single-Bit Signal Processing," *Acoustic Science and Tech,* vol. 30, pp. 429-438, 2009.